Sufficient condition for the existence of interface states in some two-dimensional photonic crystals

Xueqin Huang, Meng Xiao, Zhao-Qing Zhang, and C. T. Chan*

Department of Physics and Institute for Advanced Study, Hong Kong University of Science and Technology, Clear Water Bay, Hong Kong, China

(Received 6 March 2014; revised manuscript received 12 July 2014; published 22 August 2014)

There is no assurance that interface states can be found at the boundary separating two materials. While a strong perturbation typically favors wave localization, we show on the contrary that in some two-dimensional photonic crystals (PCs) possessing a Dirac-like cone at $\mathbf{k} = 0$ derived from monopole and dipoles excitation, a small perturbation is sufficient to create interface states. The conical dispersion together with the flat band at the zone center generates the existence of gaps in the projected band structure and the existence of single mode interface states inside the projected band gaps stems from the geometric phases of the bulk bands. The underlying physics for the existence of an interface state is related to the sign change of the surface impedance in the gaps above and below the flat band. The established results are applicable for long wavelength regimes where there is only one propagating diffraction order for an interlayer scattering.

DOI: 10.1103/PhysRevB.90.075423 PACS number(s): 42.70.Qs, 42.25.−p, 78.67.Pt, 78.68.+m

Conical dispersions in periodic systems can give rise to many properties in electronic and classical wave systems [1–7]. The most famous example is graphene's Dirac cones at the corner of the Brillouin zone [1–3]. It was shown recently that conical dispersions can also be realized at $\mathbf{k} = 0$ in two-dimensional (2D) photonic and phononic crystals [8–12]. Using effective medium theory, such 2D PCs have been shown to possess effective $\varepsilon = \mu = 0$ at the frequency of a Dirac-like point. Many interesting phenomena such as wave tunneling through arbitrary-shaped waveguides, transforming wavefronts, and cloaking [13–21] can be achieved by using 2D PCs with conical dispersion at $\mathbf{k} = 0$ [11].

In this paper we show that conical dispersion at $\mathbf{k} = 0$ can give rise to interface states in a deterministic manner. The TM polarized bulk band structure, with an electric field along the cylinder axis of a PC with C_{4v} symmetry [shown schematically in the inset of Fig. 1(a)], possessing a conical dispersion at $\mathbf{k} = 0$, is shown in Fig. 1(a). The dispersion has a upper cone and lower cone meeting at a point with $f = 0.541c/a$. Here c is the speed of light in vacuum, and a is the lattice constant. There is an additional band that is flat near $\mathbf{k} = 0$. The states in this flat band are quasilongitudinal, with the average $\mathbf{H}$ field parallel to $\mathbf{k}$ [11]. The projected band structure with $k_{||}$ along [01] (or [10]) direction is shown in Fig. 1(b). The conical dispersion guarantees that there are gaps in the projected band structure both above and below the Dirac-like point, separated by the allowed states originating from the quasilongitudinal band. We will show that the gaps above and below the quasilongitudinal bands have "opposite characters" stemming from the geometric properties of the bulk bands. These properties guarantee the existence of interface states along the [01] direction in the boundary formed between two PCs which have their system parameters slightly perturbed from the accidental degeneracy condition required for conical dispersion. Single-mode interface states will always appear in certain gap regions shared by the two PCs. The dispersions of these interface states can be predicted by calculating the surface impedance of each semi-infinite PC using scattering theory. The sign of the surface impedance (which determines the existence of the interface states) is determined by the geometric phases of the bulk photonic bands. Our results demonstrate that the surface scattering and the geometric properties of the photonic dispersion of the bulk periodic crystal are related and such knowledge can facilitate the design of localized interface modes in classical wave systems.

Our system is shown schematically in Fig. 2(a). Two semi-infinite PCs comprising dielectric cylinders in a square lattice with the same lattice constant a are put together to construct an interface along the y direction ([01] direction). The relative permittivities and radii of cylinders PCs on the left half space (red) and right half space (blue) are ε_1, R_1 and ε_2, R_2, respectively. The relative permeability is always $\mu = 1$. The bulk photonic band structures of the two PCs for TM polarization with $\varepsilon_1 = 10, R_1 = 0.205a$ and $\varepsilon_2 = 12.5, R_2 = 0.22a$ are shown in Fig. 2(b). These parameters are chosen to be slightly perturbed from the conical dispersion formation condition at $\mathbf{k} = 0$, which is $\varepsilon = 12.5, R = 0.2a$. The perturbation breaks the triply degenerate states at $\mathbf{k} = 0$ into a pair of doubly degenerate states and a singlet state. The projected band structures of the two PCs along the y direction are shown in Fig. 2(c). Pass band regions are marked in red or blue for each PC and band gaps are in white. There exist a few regions of common gaps for both projected band structures.

To search for the possibility of interface states inside the regions of common gaps, we have calculated the eigenmodes of a large slab consisting of the two PCs by the full wave numerical solver COMSOL, each with 15 cylinders along the x direction. Perfectly matched layer boundary conditions are applied to the x direction, whereas a periodic boundary condition is applied to the y direction for each wave vector $k_{||}$ along the $\bar{\Gamma}\bar{X}$ direction. In two regions of common gaps, we found single-mode interface states near the frequencies $0.53c/a$ and $0.45c/a$. These interface states are marked by green lines in Fig. 2(c). In Fig. 2(d) we plot the $\mathbf{E}$ field distribution of a typical interface mode in the upper branch marked by a black star on the green line. It is obvious that the interface state is localized near the interface. We found that as long as the structural parameters of PCs on either side of the interface are slightly perturbed relative to the conical

*Corresponding author: phchan@ust.hk

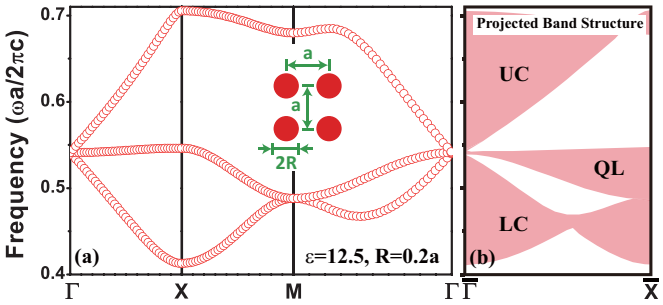

FIG. 1. (Color online) (a) The bulk band structure for $\varepsilon = 12.5, R = 0.2a$. The linear bands meeting at $\mathbf{k} = 0$ has a conical dispersion and a quasilongitudinal band that is flat along ΓX. The inset is a schematic picture of a 2D PC consisting of an array of dielectric cylinders. (b) The projected band structure for $k_{||}$ along the [01] direction. Bulk allowed states are shaded in red. The symbols UC, LC, and QL label the projected bands that are derived from the bulk bands in the upper cone, lower cone, and the quasilongitudinal bands, respectively. White marks gaps where surface states can form. The conical dispersion guarantees that there are gaps in the projected band structure above and below the bulk allowed states generated by the flat quasilongitudinal band (labeled by QL).

dispersion formation condition, the existence of interface states is assured independent of the details of the perturbation. (See Appendix A for interface state formation for different types of perturbation.)

The results of interface states shown above raise an interesting question. Why should a small perturbation near the Dirac-like cone at $\mathbf{k} = 0$ give rise to interface states and why should such localized states exist deterministically in certain common gaps but absent in others? To answer this question, we first note that the condition for the formation of an interface state is given by $Z_L(\omega,k_{||}) + Z_R(\omega,k_{||}) = 0$ [22], where $Z_{L(R)}(\omega,k_{||})$ is the surface impedance of the semi-infinite PC on the left (right) for a given $k_{||}$ [23]. In order to obtain the surface impedance, we use scattering theory [22,23] and treat the 2D PC as a large stack of one-dimensional (1D) PCs with each 1D layer having the configuration shown in Fig. 9(a) of Appendix B. Scattering theory allows us to calculate the reflection (r) and transmission (t) coefficients for this one-layer PC with an incident wave at a given frequency and $k_{||}$. The r and t for a particular value of $k_{||}$ determine an impedance for that $k_{||}$, which we will call $Z_1(\omega,k_{||})$ with the subscript "1" denoting the impedance obtained by considering one constituent layer. If we consider only the monopole and dipole bands, the reflection and transmission coefficients of a one-layer PC illuminated by an external plane wave with a given $k_{||}$ can be obtained analytically (Appendix B). The calculated r and t allow us to obtain an impedance $Z_1(\omega,k_{||}) = \pm\sqrt{(r+1)^2 - t^2}/[\sqrt{1 - k_{||}^2/k_0^2}\sqrt{(r-1)^2 - t^2}]$ for a single layer. The sign of $Z_1(\omega,k_{||})$ can be determined by the causality considerations. The projected band structures calculated with only zero-order interlayer diffraction agree well with the "exact" result computed using full-wave calculations (Appendix B) in our interested frequency region near the Dirac-like cone frequency. The projected band structures of two PCs with $\varepsilon_1 = 10, R_1 = 0.205a$ and $\varepsilon_2 = 12.5, R_2 = 0.22a$ calculated by scattering theory with only zero-order interlayer diffraction are shown in Figs. 3(a) and 3(b). Regions in which higher order diffractions play an important role are shaded in purple in Figs. 3(a) and 3(b).

We can also extract the impedance for a N-layer stack, $Z_N(\omega,k_{||})$, by calculating the r and t for a stack of N layers. As the system has inversion symmetry, we can always choose a centrosymmetric unit cell. We calculate the r and t at the boundary of the unit cell from which we determine the impedance parameter $Z_N(\omega,k_{||})$. It can be shown that $Z_N(\omega,k_{||})$ is uniquely defined and has the same value for any number of N from $N = 1$ to ∞, which will simply be denoted as $Z(\omega,k_{||})$ as long as we consider only zero-order interlayer diffraction (Appendix B). Therefore, as $Z(\omega,k_{||}) = Z_N(\omega,k_{||})$

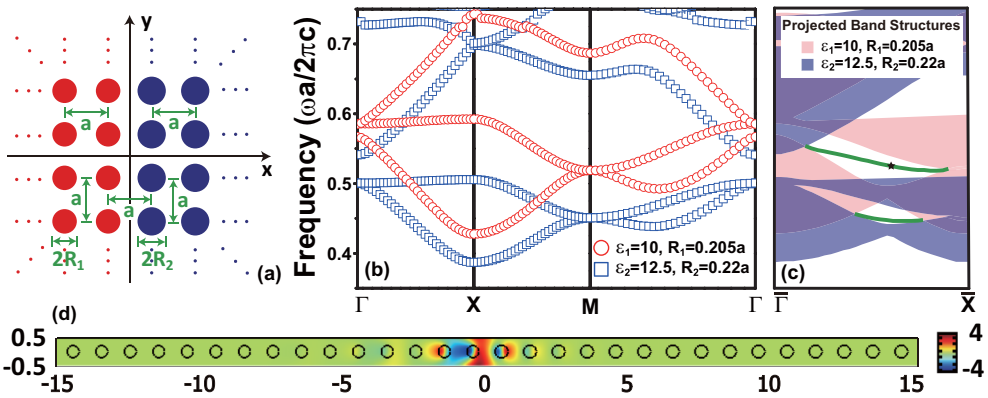

FIG. 2. (Color online) (a) Schematic picture of an interface along the [01] direction constructed by two semi-infinite 2D PCs with a square lattice. The lattice constant for both PCs are a. (b) The band structures of 2D PCs with parameters that are close to the conical dispersion condition at $\mathbf{k} = 0$. The red circles are for the PC with $\varepsilon_1 = 10, R_1 = 0.205a$, the blue squares for the PC with $\varepsilon_2 = 12.5, R_2 = 0.22a$. (c) The projected band structures of these two PCs along the interface direction ($\bar{\Gamma}\bar{X}$) with red color for the PC with $\varepsilon_1 = 10, R_1 = 0.205a$ and blue color for the PC with $\varepsilon_2 = 12.5, R_2 = 0.22a$. The green lines are the interface states. (d) The electric field distribution of the eigenmode of one interface state at the frequency $0.524c/a$ and $k_{||} = 0.6\pi/a$ [labeled by a black star on the green line in (b)] computed by COMSOL. The eigenmode is seen to be localized at x = 0 which marks the interface separating two PCs each modeled by a 15-layer slab. In the COMSOL computation, periodic boundary condition is applied along the y direction. The far ends of the unit cells are terminated by perfectly matched layers in the x direction.

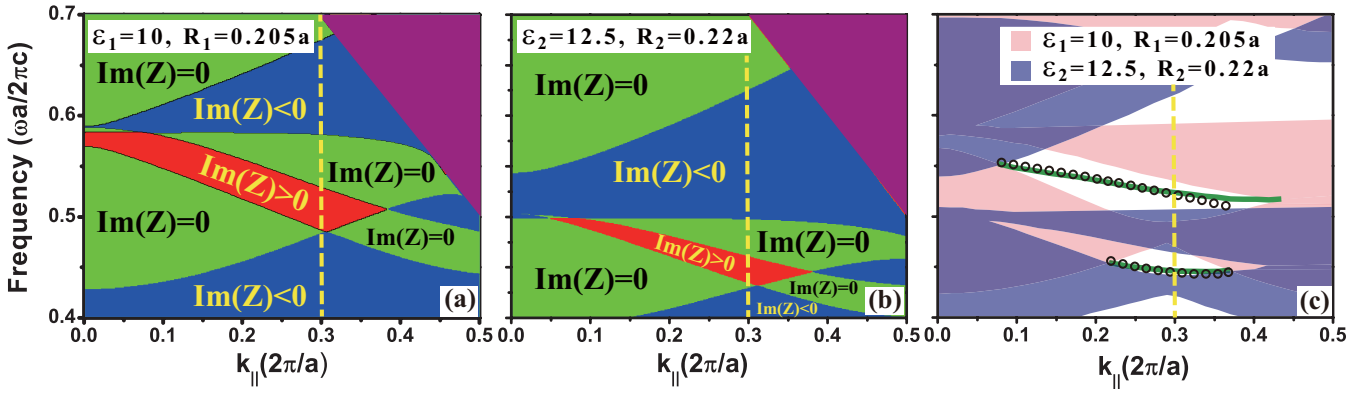

FIG. 3. (Color online) The pass and forbidden band regions in the projected band structures along the interface direction ($\bar{\Gamma}\bar{X}$) labeled with the imaginary part of the surface impedance [Im (Z)], calculated using scattering theory (ignoring interlayer evanescent coupling, see text) for (a) $\varepsilon_1 = 10, R_1 = 0.205a$ and (b) $\varepsilon_2 = 12.5, R_2 = 0.22a$. The purple color marks regions where higher order diffractions play an important role in scattering theory. (c) The projected band structures and interface states calculated by full-wave (COMSOL) calculation. Green lines represent the interface states determined using COMSOL. Black circles are calculated analytically by surface impedance shown in (a) and (b). The dashed line marks for $k_{||} = 0.6\pi/a$.

as $N \to \infty$, $Z(\omega,k_{||})$ becomes the surface impedance of the semi-infinite PC for frequencies inside the band gap and for that specific orientation as determined by the layer stacking. Therefore, the surface impedance of a semi-infinite PC $Z(\omega,k_{||})$ can be extracted from the scattering theory of just one bulk layer.

We emphasize that the surface impedance parameter is uniquely defined as long as the zero-order interlayer scattering approximation is valid. In lossless materials, $Z(\omega,k_{||})$ is pure imaginary inside a gap, i.e., $\mathrm{Im}(Z(\omega,k_{||})) > 0$ or $\mathrm{Im}(Z(\omega,k_{||})) < 0$. Figures 3(a) and 3(b) show that different gaps near the Dirac-like cone frequency carry different signs of $\mathrm{Im}(Z(\omega,k_{||}))$ and the sign can be used to characterize the gap. In particular, we note that for a given $k_{||}$, the gaps above and below the quasilongitudinal band always have a different sign of $\mathrm{Im}(Z(\omega,k_{||}))$. For a given $k_{||}$, the value of $\mathrm{Im}(Z(\omega,k_{||}))$ decreases monotonically from 0 to $-\infty$ with increasing frequency in a region with $\mathrm{Im}(Z(\omega,k_{||})) < 0$, whereas the value of $\mathrm{Im}(Z(\omega,k_{||}))$ decreases monotonically from $+\infty$ to 0 with increasing frequency in a region with $\mathrm{Im}(Z(\omega,k_{||})) > 0$. This property, together with interface state formation condition of $\mathrm{Im}(Z_L) + \mathrm{Im}(Z_R) = 0$ implies that there must exist one and only one interface state inside the common gap if the surface impedances of the two 2D PCs have different signs and therefore cannot be interface states inside the gap if $\mathrm{Im}(Z_L)$ and $\mathrm{Im}(Z_R)$ have the same sign. In Figs. 3(a) and 3(b) we mark explicitly the sign of $\mathrm{Im}(Z(\omega,k_{||}))$ in each gap of the two PCs. According to the condition of interface state formation, it is easy to see that there are interface states in the common gaps with frequencies around $0.53c/a$ and $0.45c/a$, whereas no interface states are allowed in the other common gaps. In addition, we can use the value of $\mathrm{Im}(Z(\omega,k_{||}))$ extracted from the scattering theory to calculate the interface wave dispersions. The results are shown as black circles in Fig. 3(c). For comparison we have also carried out the full-wave (COMSOL) calculations to obtain the band dispersions of the interface states. These results are shown by green lines in Fig. 3(c). Excellent agreements have been found between the two calculations.

The guaranteed existence of surface or interface states is frequently related to the topological properties of the bulk bands [24–35]. To give an "geometric" interpretation of the formation of interface states, we note that the projected band structure for a particular $k_{||}$ comes from the bulk bands with a fixed $k_y = k_{||}$ and with k_x varying from $-\pi/a$ to π/a. For example, the pass bands and forbidden gaps in the projected band structure at $k_{||} = 0.6\pi/a$ in Fig. 3(c) (marked by a yellow dashed line) correspond to reduced 1D band structures shown in Fig. 4, where we plot the reduced 1D band structures of two PCs along the k_x direction with $k_y = 0.6\pi/a$ and $\varepsilon_1 = 10, R_1 = 0.205a$, and $\varepsilon_2 = 12.5, R_2 = 0.22a$, respectively.

We calculate the geometric Zak phase [36] of the reduced 1D bands shown in Fig. 4 using the formula

$$\varphi_n = i \int_{-\pi/a}^{\pi/a} \langle u_{nk_x,k_y=k_{||}} | \varepsilon(\vec{r}) \partial_{k_x} | u_{nk_x,k_y=k_{||}} \rangle dk_x, \qquad (1)$$

where $u_{n\vec{k}}$ is the cell periodic part of the Bloch function of the $\mathbf{E}$ field for the nth band at a particular $\vec{k}$, and $\varepsilon(\vec{r})$ is position dependent relative permittivity. The Zak phase is calculated using the periodic gauge and the origin is chosen at the left boundary of the unit cell as shown in the right panel in Fig. 4(a). The Zak phases for the four lowest bands are $\varphi_1 = \pi$ and $\varphi_n = 0$ for $n = 2, 3, 4$. The zero Zak phases of bands 2 and 3 are required by the C_{4v} symmetry of the PCs (Appendixes C and D). Now we apply a rigorous relation found in a 1D system with inversion symmetry [37]. The relation relates the ratio of the signs of $\mathrm{Im}(Z(\omega,k_{||}))$ in two adjacent gaps, say the nth and $(n-1)$th gaps, to the Zak phase of the band in between [37], i.e.,

$$\frac{\mathrm{Sgn}[\mathrm{Im}(Z_n(\omega,k_{||}))]}{\mathrm{Sgn}[\mathrm{Im}(Z_{n-1}(\omega,k_{||}))]} = e^{i(\varphi_{n-1}+\pi)}. \qquad (2)$$

One point we want to note is that Eq. (2) is valid for only considering the monopole and dipole bands with zero-order interlayer diffraction. It is easy to show that the sign of $\mathrm{Im}(Z(\omega,k_{||}))$ in the lowest gap is always negative. The knowledge of the Zak phases of the bulk bands allows us to determine the signs of the gaps through Eq. (2). The results

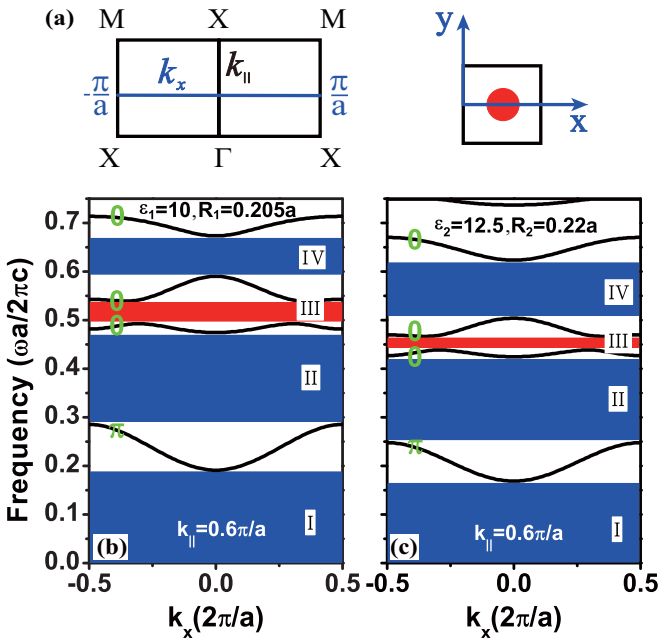

FIG. 4. (Color online) (a) Left panel denotes the Brillouin zone of a square lattice, the blue line represents k_x running from $-\pi/a$ to π/a with a fixed $k_{||}$. The right panel shows the coordinate for calculating the Zak phase, the origin is located on the left boundary of the unit cell. The bulk band structure with a fixed $k_y = k_{||} = 0.6\pi/a$ for the PC with (b) $\varepsilon_1 = 10, R_1 = 0.205a$ and (c) $\varepsilon_2 = 12.5, R_2 = 0.22a$. The Zak phases of the bulk bands are labeled with green. The characters of the bulk gaps are labeled by the sign of Im (Z) with blue color for Im $(Z) < 0$and red color for Im $(Z) > 0$.

are shown in Figs. 4(b) and 4(c), where the blue color denotes the gaps with $\mathrm{Im}(Z(\omega,k_{||})) < 0$ and the red color stands for the gaps with $\mathrm{Im}(Z(\omega,k_{||})) > 0$. These results are consistent with that of the scattering theory shown in Figs. 3(a) and 3(b) along the yellow dashed lines, respectively. Thus, for only considering the monopole and dipole bands, by knowing the bulk Zak phase we can also determine the sign of $\mathrm{Im}(Z(\omega,k_{||}))$ without doing any calculations using scattering theory. From Figs. 4(b) and 4(c) it is also seen that there are two overlapping gaps that have different signs of $\mathrm{Im}(Z(\omega,k_{||}))$. The overlap of the second gap in Fig. 4(b) and the third gap in Fig. 4(c) gives rise to the lower branch of the interface states near the frequency $0.45c/a$ found in Fig. 3(c) and the overlap of the third gap in Fig. 4(b) and the fourth gap in Fig. 4(c) gives rise to the higher branch near the frequency $0.53c/a$.

We note that there is in general no assurance for the existence of interface states between two arbitrary photonic crystals. While interface states in 2D PCs have been obtained using numerical computations [38–42], it is highly desirable to explain the underlying physics of the interface state formation and to search for configurations where interface state existence is guaranteed. We show here that the Dirac-like cone at $\mathbf{k} = 0$ systems provides a systematic way to generate interface states. The conical dispersions at $\mathbf{k} = 0$ has two special properties that facilitates the formation of interface states: (1) the conical band structure provides gaps in the projected band and (2) the associated quasilongitudinal flat band (which always accompanies the conical dispersion at $\mathbf{k} = 0$) divides the gap into two regions with different signs of surface impedance. The different signs of surface impedance can be traced to the geometric properties of the bulk bands. We should point out that the presence of a Dirac-like cone is a sufficient condition for the creation of interface states but it is not a necessary condition. We emphasize that the identification of interface modes using bulk-interface correspondence [the discussion near Eqs. (1) and (2)] is not limited to Dirac-like cone systems. It is generally applicable to classical wave systems as long as the impedance is a complex number (rather than a matrix), which is correct in the subdiffraction regime we are considering. Our method of interface mode analysis, which considers the properties of the band gaps as characterized by the sign of the surface impedance and tracing the origin to bulk band geometric characteristics, can be applied to other systems as well. In fact, the physics considered here can be applied equally well to phononic systems. The physics of interface states demonstrated here can provide a useful paradigm for the construction of interface states in different classes of classical wave systems.

C.T.C. thanks Professor Feng Wang and Professor Vic Law for discussions. This work is supported by Hong Kong RGC Grants 600311 and AOE/P-02/12.

APPENDIX A: INTERFACE STATES IN TWO-DIMENSIONAL PHOTONIC CRYSTALS WITH CONICAL DISPERSIONS

In two-dimensional (2D) photonic crystals (PCs), the Dirac-like cone at $\mathbf{k} = 0$ can be formed by the accidental degeneracy of the monopole and dipole degrees of freedom [11]. The interface we are considering separates two semi-infinite 2D PCs, each with system parameters (dielectric constant and/or radius of cylinders) that are slightly perturbed from the accidental degeneracy condition to form a Dirac-like cone at the zone center. Due to the requirement of threefold degeneracy, we note that the conical dispersion at $\mathbf{k} = 0$ (accounting for 2 degrees of freedom) must coexist with an additional band whose character is quasilongitudinal and nearly dispersionless near the Dirac-like point. We note that this band is also required to exist because of the zero-index equivalence [11] as zero-index material has an additional longitudinal solution. Here we give two examples in which the frequency difference between two quasilongitudinal bands is very small as shown in Figs. 5 and 6. Figure 5 shows the case when both PCs on each side have a higher frequency for the dipole mode, whereas in Fig. 6 the monopole modes have a higher frequency. Even though the common band gap between two quasilongitudinal bands is very small for both cases, we are able to find a band of interface states in each common band gap. To visualize these interface states, we also plot in Figs. 5(c) and 6(c) two eigenmodes of two interface states at some particular $k_{||}$ (labeled by black stars on the green lines). It is clearly seen that the electric field is localized near the interfacial region in each case.

From the two examples shown above, we have demonstrated that "perturbing the conical dispersion" generates interface states. Noting that the accidental degeneracy at the conical point at $\mathbf{k} = 0$ comes from the degeneracy of a pair

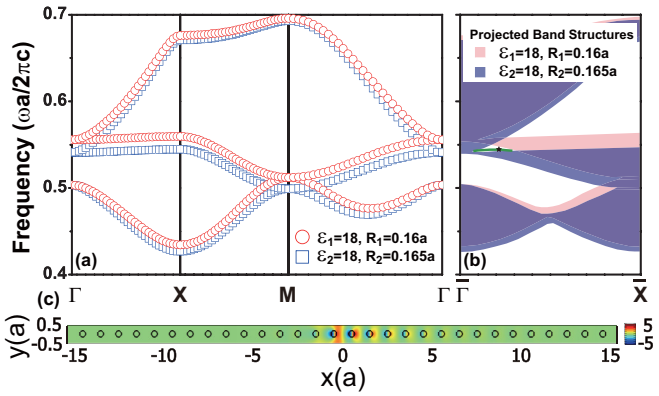

FIG. 5. (Color online) (a) The band structures of 2D PCs with parameters that are close to the conical dispersion condition at $\mathbf{k}=0$. The red circles are for the PC with $\varepsilon_1 = 18, R_1 = 0.16a$, and the blue squares for the PC with $\varepsilon_2 = 18, R_2 = 0.165a$. (b) The projected band structures of these two PCs along the interface direction ($\bar{\Gamma}\bar{X}$) with red color for the PC with $\varepsilon_1 = 18, R_1 = 0.16a$ and blue color for the PC with $\varepsilon_2 = 18, R_2 = 0.165a$. The green line in the common band gap represents the interface states. (c) The electric field distribution of the eigenmode of one interface state at the frequency $0.544c/a$ and $k_{||} = 0.22\pi/a$ [labeled by a black star on the green line in (b)] computed by COMSOL.

of doubly degenerate dipole modes and a monopole mode, perturbation will cause the splitting of the threefold degeneracy into a twofold (dipoles) and onefold (monopole) and there are three possible combinations:

(i) The monopole is higher in frequency than the dipole at $\mathbf{k}=0$ in one PC on one side of the interface and the monopole is lower in frequency than the dipole at $\mathbf{k}=0$ on another side of the interface. This case is shown in Fig. 2 of the main text.

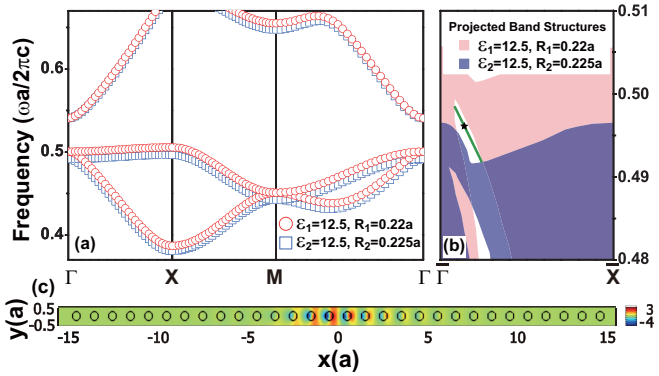

FIG. 6. (Color online) (a) The band structures of 2D PCs with parameters that are close to the conical dispersion condition at $\mathbf{k}=0$. The red circles are for the PC with $\varepsilon_1 = 12.5, R_1 = 0.22a$, and the blue squares for the PC with $\varepsilon_2 = 12.5, R_2 = 0.225a$. (b) The enlarged projected band structures of these two PCs along the interface direction ($\bar{\Gamma}\bar{X}$) with red color for the PC with $\varepsilon_1 = 12.5, R_1 = 0.22a$ and blue color for the PC with $\varepsilon_2 = 12.5, R_2 = 0.225a$. The green line in the common band gaps represents the interface states. (c) The electric field distribution of the eigenmode of one interface state at the frequency $0.496c/a$ and $k_{||} = 0.144\pi/a$ [labeled by a black star on the green line in (b)] computed by COMSOL.

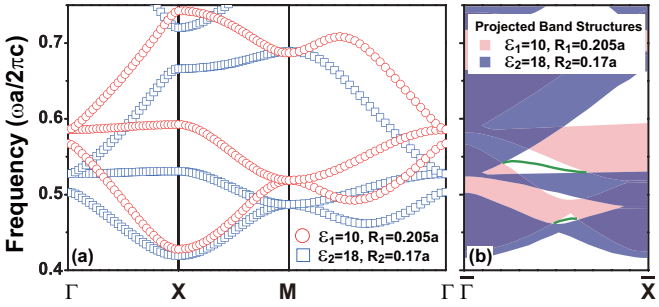

FIG. 7. (Color online) (a) The band structures of 2D PCs with parameters that are close to the conical dispersion condition at $\mathbf{k}=0$. The red circles are the band structures for the PC with $\varepsilon_1 = 10, R_1 = 0.205a$, and the blue squares for the PC with $\varepsilon_2 = 18, R_2 = 0.17a$. For both of the band structures, the frequencies of dipole bands are higher than those of the monopole bands at $\mathbf{k}=0$. (b) The projected band structures of PCs along the interface direction ($\bar{\Gamma}\bar{X}$) with red color for the PC with $\varepsilon_1 = 10, R_1 = 0.205a$ and blue color for the PC with $\varepsilon_2 = 18, R_2 = 0.17a$. There are five common band gaps in both of the two projected band structures. The green lines in the common band gaps represent the interface states at the interface created by the two PCs. Here a is the lattice constant of the PCs.

(ii) The monopole is lower in frequency than the dipole at $\mathbf{k}=0$ in both PCs (see Fig. 7 below). Figure 5 is an extreme case of this category.

(iii) The monopole is higher in frequency than the dipole at $\mathbf{k}=0$ in both PCs (see Fig. 8 below). Figure 6 is an extreme case of this category.

In Fig. 7(a) we show the case in which the frequencies of dipole bands are higher than those of monopole bands at $\mathbf{k}=0$ on both sides of the interface. The bulk band structures of two PCs have the following parameters: $\varepsilon_1 = 10, R_1 = 0.205a$ for the PC with red circles and $\varepsilon_2 = 18, R_2 = 0.17a$ for the PC

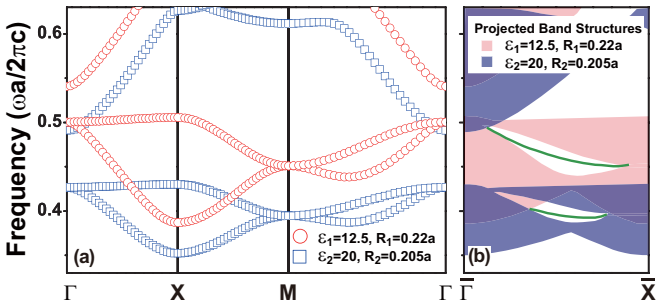

FIG. 8. (Color online) (a) The bulk band structures of two PCs with different parameters that are close to the conical dispersion condition at $\mathbf{k}=0$. The red circles are the band structures for the PC with $\varepsilon_1 = 12.5, R_1 = 0.22a$, and the blue squares for the PC with $\varepsilon_2 = 20, R_2 = 0.205a$. For both of the band structures, the frequencies of dipole bands are lower than those of the monopole bands at $\mathbf{k}=0$. (b) The projected band structures of PCs along the interface direction ($\bar{\Gamma}\bar{X}$) with red color for the PC with $\varepsilon_1 = 12.5, R_1 = 0.22a$ and blue color for the PC with $\varepsilon_2 = 20, R_2 = 0.205a$. There are four common band gaps in both of the two projected band structures. The green lines in the common band gaps represent the interface states at the interface created by the two PCs. Here a is the lattice constant of the PCs.

with blue squares. The projected band structures of two PCs along the interface direction ($\bar{\Gamma}\bar{X}$) are shown in Fig. 7(b). There are five common band gaps: the first one is near the frequency $0.625c/a$, the second one is in the frequency range between $0.526c/a$ and $0.563c/a$, i.e., the region between two quasilongitudinal flat bands in the bulk band structures of two PCs, the third one is in the range between $0.49c/a$ and $0.51c/a$, the fourth one between $0.46c/a$ and $0.48c/a$, and the fifth one is around the frequency $0.425c/a$. The interface states are found in the second and fourth common partial band gaps denoted by two green lines in Fig. 7(b). The results for the case where the frequencies of monopole bands are higher than those of dipole bands at $\mathbf{k}=0$ on either side of the interface are shown in Fig. 8. Interface states are also found.

APPENDIX B: SURFACE IMPEDANCE $Z(\omega,k_{||})$ AND SCATTERING THEORY

In order to obtain the surface impedance $Z(\omega,k_{||})$ for 2D PC, we use the layer-by-layer scattering formalism, which treats a 2D PC as stacks of 1D PCs. Detailed description of layer-by-layer scattering formalism can be found in the literature [23]. We start with one single constituent layer, which in our system is one single row of cylinders with distance a between the cylinders. The one-layer PC is arranged along the y direction with one unit cell along the x direction, and the cylinders are centered in the unit cell and at $x=a/2$ [shown in Fig. 9(a)]. Scattering theory allows us to calculate the reflection (r) and transmission (t) coefficients for this one-layer PC with an incident wave at a given frequency and $k_{||}$. If we consider only the monopole and dipole bands, the reflection and transmission coefficients of a one-layer PC illuminated by an external plane wave with a given $k_{||}$ can be obtained analytically and the results are

$$r=\frac{i}{2ak_x}(\tilde{P}+\tilde{M}_x k_{||}+\tilde{M}_y k_x)$$
$$\text{and}\quad t=\left[1+\frac{i}{2ak_x}(\tilde{P}+\tilde{M}_x k_{||}-\tilde{M}_y k_x)\right], \tag{A1}$$

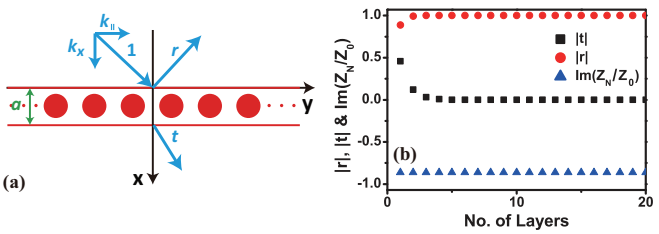

FIG. 9. (Color online) (a) The system configuration used for calculating the reflection (r) and transmission (t) coefficients for a one-layer PC. The cylinders are at the center of unit cell at $x=a/2$. (b) The moduli of reflection ($|r|$) and transmission ($|t|$) coefficients and the imaginary part of surface impedance [$\mathrm{Im}(Z_N)$] inside the band gap of a N-layer PC for considering only zero-order interlayer diffraction as a function of the number of layers of the 1D PC with a fixed $k_{||}=0.6\pi/a$. In the N-layer slab, each layer has the configuration shown in (a) with $\varepsilon_1=12.5, R_1=0.22a$. The working frequency is $0.524c/a$. Here Z_0 is the impedance of vacuum.

where $\tilde{P}=[1/\alpha_M+F_6-ik_{||}F_3]/\{[\varepsilon_0/(\alpha_E k_0^2)-F_1](1/\alpha_M+F_6)+F_3^2\}$, $\tilde{M}_x=\{-iF_3+k_{||}[\varepsilon_0/(\alpha_E k_0^2)-F_1]\}/\{[\varepsilon_0/(\alpha_E k_0^2)-F_1](1/\alpha_M+F_6)+F_3^2\}$, and $\tilde{M}_y=-k_x/(1/\alpha_M+F_4)$. Here α_E and α_M are the monopolar and dipolar polarizability of the cylinder, $k_{||}$ is the wave vector along the y direction, k_x is the wave vector perpendicular to the interface, $k_0=\omega/c$, where ω is the angular frequency, and F_1, F_3, F_4, F_6 are 1D lattice sums defined as

$$F_1=\sum_{m\neq 0}\frac{i}{4}H_0(k_0|\vec{r}-ma\hat{y}|)e^{imk_{||}a}\Big|_{\vec{r}=0},$$
$$F_3=\frac{\partial}{\partial y}\sum_{m\neq 0}\frac{i}{4}H_0(k_0|\vec{r}-ma\hat{y}|)e^{imk_{||}a}\Big|_{\vec{r}=0},$$
$$F_4=\frac{\partial^2}{\partial x^2}\sum_{m\neq 0}\frac{i}{4}H_0(k_0|\vec{r}-ma\hat{y}|)e^{imk_{||}a}\Big|_{\vec{r}=0}, \tag{A2}$$
$$F_6=\frac{\partial^2}{\partial y^2}\sum_{m\neq 0}\frac{i}{4}H_0(k_0|\vec{r}-ma\hat{y}|)e^{imk_{||}a}\Big|_{\vec{r}=0},$$

where m is an integer, and $H_0(x)$ is the zero-order Hankel function of the first kind. The r and t for a particular value of $k_{||}$ determine an impedance for that $k_{||}$, which we will call $Z_1(\omega,k_{||})$ with the subscript "1" denoting the impedance obtained by considering one constituent layer shown in Fig. 9(a).

We can extract the impedance for a N-layer stack by calculating the r and t for a stack of N layers, and let those be denoted by $Z_N(\omega,k_{||})$. As the system has inversion symmetry, we can always choose a centrosymmetric unit cell. We determine the r and t at the boundary of the unit cell from which we determine the impedance parameter $Z_N(\omega,k_{||})$. For the frequencies and k vectors we are considering, it is sufficient to consider only zero-order interlayer diffraction, namely that the evanescent wave coupling between adjacent layers can be ignored. It can be shown that $Z_N(\omega,k_{||})$ is uniquely defined and has the same value for any number of N from $N=1$ to ∞ which will simply be denoted as $Z(\omega,k_{||})$. In Fig. 9(b) we show the moduli of reflection ($|r|$) and transmission ($|t|$) coefficients inside the band gap with fixed $k_{||}=0.6\pi/a$ and $f=0.524c/a$ as function of the number of N of the 1D PC with only zero-order interlayer diffraction included. Each layer of PC has the configuration shown in Fig. 9(a) with $\varepsilon_1=12.5, R_1=0.22a$. Although $|r|$ and $|t|$ are dependent on N, and each converges to a constant when N is large, $Z_N(\omega,k_{||})$ is independent of N. Therefore, as $Z(\omega,k_{||})=Z_N(\omega,k_{||})$ as $N\to\infty$, $Z(\omega,k_{||})$ becomes the surface impedance of the semi-infinite PC for frequencies inside the band gap and for that specific orientation as determined by the layer stacking. Therefore, the surface impedance of a semi-infinite PC $Z(\omega,k_{||})$ can be obtained from the scattering theory of just one bulk layer.

We note the surface impedance $Z(\omega,k_{||})$ is extracted via calculating the reflection (r) and transmission (t) coefficients of the one-layer PC and as such, it ignores evancesent waves. This is a good approximation if high-order interlayer diffractions can be ignored. To verify whether only considering the zero-order interlayer diffraction is adequate, we calculate

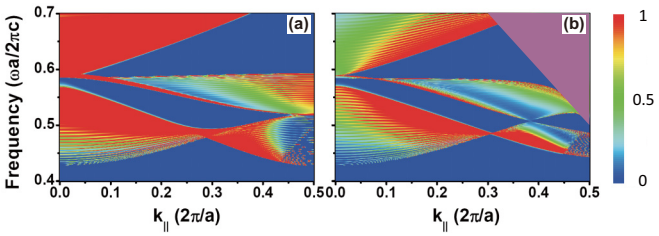

FIG. 10. (Color online) The projected band structures of PC along the interface direction ($\bar{\Gamma}\bar{X}$) with $\varepsilon_1 = 10, R_1 = 0.205a$ calculated by two different methods: (a) for full-wave calculation and (b) for multiple scattering theory with only zero-order interlayer diffraction. The purple region in (b) represents the higher-order diffractions play an important role in the multiple scattering theory.

the projected band structure of one PC along the interface direction ($\bar{\Gamma}\bar{X}$) and compare the result of the full wave calculation with that if high-order interlayer diffraction can be ignored. The relative permittivity, permeability, and radius of the cylinders of the PC are $\varepsilon_1 = 10, R_1 = 0.205a$, respectively. The full-wave calculation is shown in Fig. 10(a) and the calculation obtained by scattering theory for only zero-order interlayer diffraction is shown in Fig. 10(b). The purple region shown in Fig. 10(b) is the region where the higher-order diffractions should play an important role and we see that the results of these two methods agree well with each other for a large region of $k_{||}$.

APPENDIX C: CALCULATIONS OF THE ZAK PHASES

In the main text we use the numerical calculations to evaluate the Zak phases of certain reduced 1D bands for a particular $k_{||}$. In this Appendix we show the details about how to calculate the Zak phase and use the method proposed by Kohn [43] to verify the Zak phase obtained by numerical calculations.

In 2D PC, the Bloch wave vector comprises k_x and k_y, in order to get the projected band structure, we fix $k_y = k_{||}$ and let k_x vary from $-\pi/a$ to π/a. In the main text we have plotted the bulk band structures of two PCs along the k_x direction for $k_y = 0.6\pi/a$ (shown in Fig. 4). The definition of Zak phase in 1D is $\varphi_n = i\int_{-\pi/a}^{\pi/a} \langle u_{nk_x,k_y=k_{||}} | \varepsilon(\vec{r}) \partial_{k_x} | u_{nk_x,k_y=k_{||}} \rangle dk_x$ [36], where $u_{n\vec{k}}$ is the cell periodic part of the Bloch function of the E field for the nth band at a particular $\vec{k}$, and $\varepsilon(\vec{r})$ is position dependent relative permittivity in the unit cell. For the implement of numerical calculations, the integral formula has been changed to summation form, so $\varphi_n = -\sum_{l=1}^{M} \mathrm{Im} \ln \langle u_{nk_{x,l},k_y=k_{||}} | \varepsilon(\vec{r}) | u_{nk_{x,l+1},k_y=k_{||}} \rangle$ in the limit of large M [44]. For TM polarization (E along cylinder axis direction), the eigenmodes of $E_{n\vec{k}}$ and $u_{n\vec{k}}$ are related by $E_{n\vec{k}}(\vec{r}) = u_{n\vec{k}}(\vec{r}) \exp(i\vec{k}\cdot\vec{r})$. To obtain the Zak phases of these bands, we first use COMSOL to calculate the eigenmodes $u_{n\vec{k}}(\vec{r})$ of 2D PC for different k_x at a particular nth band and $k_y = k_{||}$. Then, we can calculate the inner product: $\langle u_{nk_{x,l},k_y=k_{||}} | \varepsilon(\vec{r}) | u_{nk_{x,l+1},k_y=k_{||}} \rangle = \iint_{\text{unit cell}} \varepsilon(\vec{r}) u^*_{nk_{x,l},k_y=k_{||}}(\vec{r}) \cdot u_{nk_{x,l+1},k_y=k_{||}}(\vec{r}) d\vec{r}$. With this inner product, using the periodic gauge $u_{n,-\pi/a,k_y}(x,y) = \exp(i2\pi x/a) u_{n,\pi/a,k_y}(x,y)$, the Zak phase of the nth band can be obtained (shown in Fig. 4). Since the Zak phase is dependent on the choice of the origin, in the calculation we set the origin at the left boundary of the unit cell (shown in Fig. 4).

We will use the method given by Kohn [43] to determine the Zak phases of the bulk bands. Noting that our system possesses inversion symmetry and in the subdiffraction regime we have effectively an 1D problem after fixing a $k_y = k_{||}$, the Zak phase of the band should be π if the eigenmodes at the two high symmetry points in the Brillouin zone have different symmetries [43], and it should be zero otherwise. These two high symmetry points in the reciprocal space are the P ($k_x = 0, k_y = k_{||}$) and Q ($k_x = -\pi/a, k_y = k_{||}$) points shown in Fig. 11(a). We choose the origin of the coordinate to be at the center of the cylinder, the unit cell chosen in this way is different from the case depicted Fig. 4 in the main text. We plot the eigenmodes (E_z field) of P and Q points in Fig. 11. The real part and imaginary part of the eigenmodes represent the interactions between monopole and dipole excitations. Since the system at P and Q points possess σ_x mirror symmetry, the real part and imaginary part of the eigenmodes should be either an even or odd function of x. Through analyzing the mirror symmetry of the eigenmodes at P and Q points, we can obtain the Zak phases of the bands. Let us first examine the eigenmodes of the quasilongitudinal band (the third band in the band structure shown in Fig. 4) at the P point. The real part and imaginary part of the eigenmode are antisymmetric [shown in Figs. 11(b) and 11(c)]. At the Q point, the real part and imaginary part of the eigenmode are symmetric [shown in Figs. 11(d) and 11(e)]. Based on the criterion given by Kohn, the Zak phase for the quasilongitudinal band is π. The same analysis shows that the Zak phase for the lower band (the second band in the band structure shown in Fig. 4) is also equal to π. The Zak phase is dependent on the choice of the origin. If we choose the origin of the coordinate in the middle of two nearest neighbor cylinders (as shown in Fig. 4 in the main text), all the Zak phases of the bands discussed above should have an addition phase of π. Therefore, both the Zak phases of the second and third bands discussed in the main text should be 0.

APPENDIX D: THE GROUP THEORY ANALYSIS FOR THE ZAK PHASES OF THE REDUCED 1D BANDS AND THE FORMATION OF INTERFACE STATES

Here we analyze the problem from a group theory point of view. The group theoretical technique is given in detail in Sakoda's book [45]. To be consistent with the conventional group theory treatment [45], we choose here the origin of the coordinate to be at the center of the cylinder [shown in Fig. 12(a)]. This choice is different from the origin chosen in the Zak phases calculations in Fig. 4 (at the middle of two neighboring cylinders), which was more convenient for scattering theory treatment. We note that there is a phase shift of π due to this shift of origin. Thus, to prove that the Zak phases of the three lowest bands shown in Fig. 4 are π, 0, 0, here we need to show that the Zak phases of the three lowest bands to be 0, π, π if the origin is chosen at the cylinder centers.

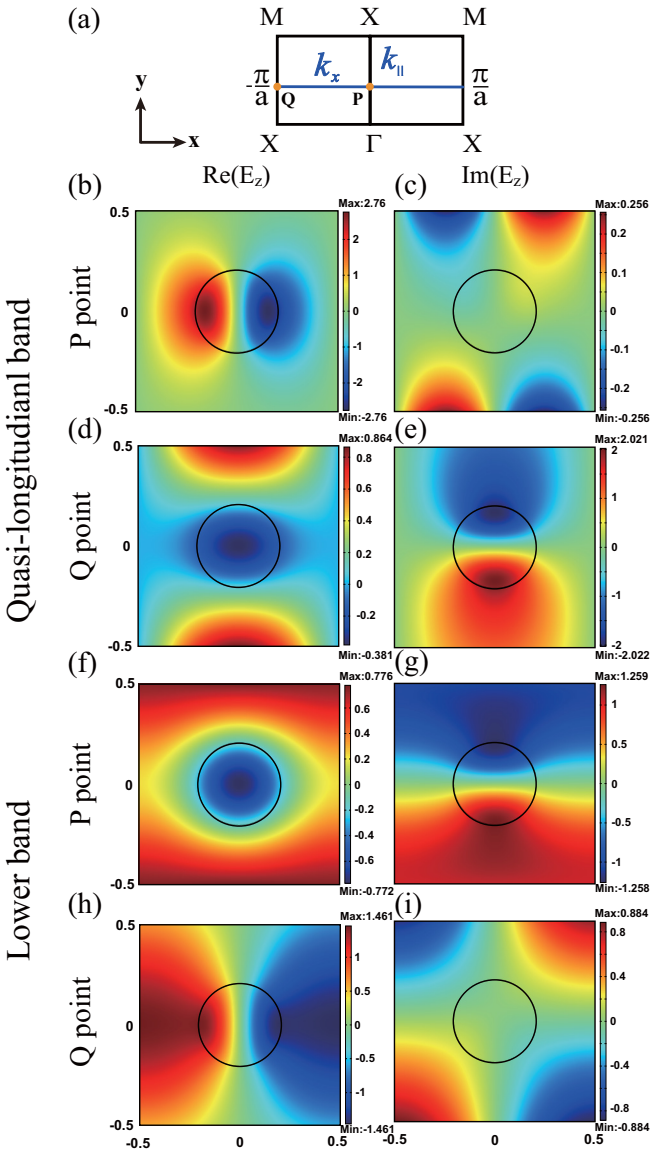

FIG. 11. (Color online) The electric field distributions of the eigenmodes at two high symmetry points for two bands in a unit cell. (a) The schematic of k_x from $-\pi/a$ to $\pi/a$with a fixed $k_{||}$in the Brillouin zone. The relative permittivity, permeability, and radius of the cylinders of the PC are $\varepsilon_1 = 10, R_1 = 0.205a$, respectively. Here a is the lattice constant. $\boldsymbol{P}$ and $\boldsymbol{Q}$ points denote two high symmetry points in the Brillouin zone. (b), (c) and (d), (e) are the electric field distributions of the eigenmodes in $\boldsymbol{P}$ and $\boldsymbol{Q}$ points for the quasilongitudinal band (the third band in the band structure shown in Fig. 4), respectively. (f), (g) and (h), (i) are the electric field distributions of the eigenmodes in $\boldsymbol{P}$ and $\boldsymbol{Q}$ points for the lower band (the second band in the band structure shown in Fig. 4), respectively. The origin of the coordinate is located at the center of the cylinder.

In the left panel of Fig. 12(a) we show the 2D Brillouin zone of the photonic crystal which has C_{4v} symmetry. To study interface states with a fixed $k_{||}$, we need to consider the reduced 1D Brillouin zone (BZ) by fixing $k_y = k_{||}$ and let k_x vary from $-\pi/a$ to π/a as shown with the blue line. The zone center and boundary points in this reduced 1D Brillouin zone are labeled by P $(k_x = 0, k_y = k_{||})$ and Q $(k_x = -\pi/a, k_y = k_{||})$, respectively.

The cylinder is located at the center of the unit cell. The origin of the coordinate is also chosen at the center of the cylinder as shown in the right panel of Fig. 12(a). Following the procedures detailed in Ref. [45], the irreducible representations of the bands along the high symmetry points and lines of the 2D BZ can be found and they are shown in Fig. 12(b) for the PC with $\varepsilon = 10, R = 0.205a$ and $k_{||} = 0.2\pi/a$. In the following we give some details of the symmetry of the low lying bands relevant for our study. The third band is a quasilongitudinal band along ΓX. The average magnetic field is parallel to the wave vector and the eigenelectric field has odd symmetry with respect to the direction of the wave vector. The P_3 point shown in Fig. 12(b) is the eigenmode of the third band with wave vector at the P point [shown in Fig. 12(a)]. As it is a quasilongitudinal mode with wave vector along the y direction, it has odd symmetry under σ_x, and so it has the B representation. At X' point $(k_x = -\pi/a, k_y = 0)$, the quasilongitudinal mode should have different (odd or even) symmetries under σ_x and σ_y, it can hence be represented by the B_1 or B_2 representation. Since the quasilongitudinal mode along the $\Gamma X'$ direction is odd under σ_y, it has B_2 representation. The compatibility relation requires that the mode with B_2 representation along the $X'M$ direction $(k_x = -\pi/a, k_y)$ has even symmetry under σ_x, which has A representation. So the eigenmode of the Q_3 point shown in Fig. 12(b) has even symmetry under σ_x. The eigenmodes of the P_3 and Q_3 points in the third band have opposite symmetries under σ_x, and as such, the Zak phase of this band should be π with respect to the origin of the coordinate located at the center of the cylinder [shown in the right panel of Fig. 12(a)]. If the origin of the coordinate is chosen to be in the middle of two neighbor cylinders, the Zak phase should be added with π, then it becomes 0 [shown in Fig. 12(c)]. With similar arguments we can obtain the representations of the eigenmode of the first and second bands at the P and Q points shown in Fig. 12(b). We can then also obtain the Zak phases of these bands shown in Fig. 12(c).

From Eq. (2) in the main text, we showed that the signs of the surface impedances of the projected band gaps above and below the flat band manifold must be opposite as required by the symmetry of the system. If the interface is formed by two PCs with parameters that are slightly perturbed from those of a Dirac-like cone, there is a common gap. This is quite obvious already in Figs. 2(b), 3(c), 5(b), 6(b), 7(b), and 8(b). This situation is further illustrated schematically in Fig. 12(d), where the common gap is between two dashed black lines in Fig. 12(d)). It is in this common gap region that interface modes decaying exponentially into the bulk can form. We note in particular that for one of the PC (red color), the common gap is *below* the projected band of the flat band of that PC derived from the quasilongitudinal bands, while for the other PC (blue color), the common gap is *above* the projected band of the flat band of the other PC. That is to say, in the common gap, one PC on one side of the interface must have an opposite sign of surface impedance to the PC on the other side. As a consequence, one interface state should exist in this gap.

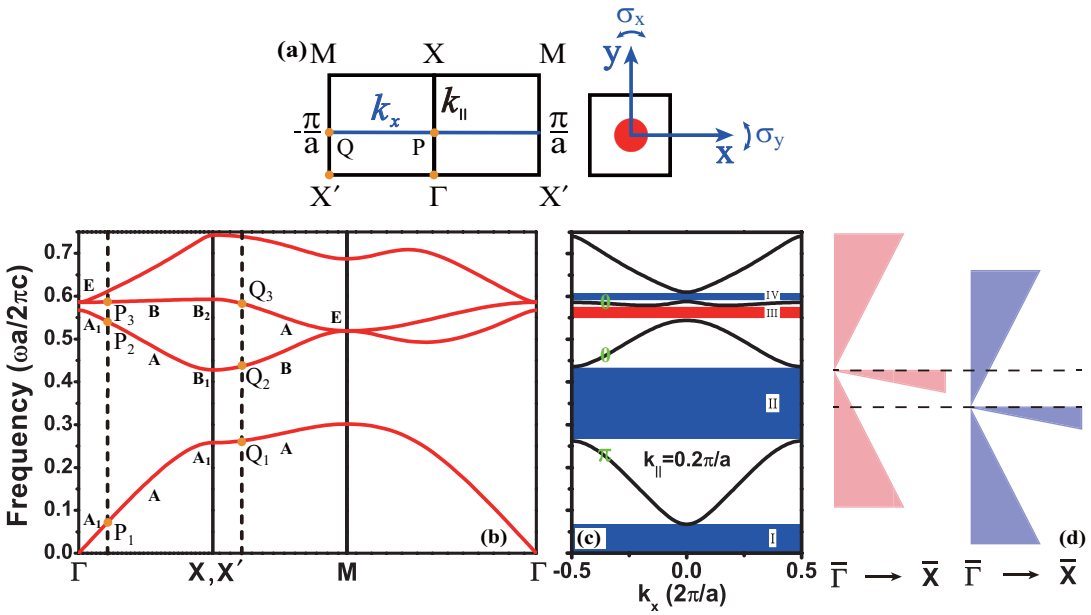

FIG. 12. (Color online) (a) The left panel shows the 2D Brillouin zone. The blue line marks the reduced 1D zone along the k_x direction for a fixed $k_y = k_{||}$ with the k points P and Q at the center and the boundary, respectively. The right panel shows one unit cell of the 2D PC with the origin of the coordinate at the center of the unit cell. (b) The bulk band structure of the PC with $\varepsilon = 10, R = 0.205a$. The two dashed black lines denote wave vector $k_y = k_{||} = 0.2\pi/a$ along the ΓX and $X'M$ directions, respectively. P_1, P_2, and P_3 denote the eigenmodes in the first, second, and third bands with wave vector at P point shown in (a) with $k_y = k_{||} = 0.2\pi/a$, respectively. Q_1, Q_2, and Q_3 denote the eigenmodes in the first, second, and third bands with wave vector at Q point shown in (a) with $k_y = k_{||} = 0.2\pi/a$, respectively. (c) The Zak phases of the three lowest bands for the PC with $\varepsilon = 10, R = 0.205a$ and $k_{||} = 0.2\pi/a$ are labeled with green. Here the origin of the coordinate for calculating the Zak phase is located in the middle of two neighbor cylinders (the same as Fig. 4). The characters of the bulk gaps are labeled by the sign of $\mathrm{Im}(Z)$ with blue color for $\mathrm{Im}(Z) < 0$ and red color for $\mathrm{Im}(Z) > 0$. (d) The schematic diagram showing the projected bands of two PCs along the $\bar{\Gamma}\bar{X}$ direction with two Dirac-like cones with a small frequency deviation. There is a common gap (between two dashed black lines) between the projected bands of the two flat bands.

APPENDIX E: THE RELATIONSHIP OF THE SURFACE IMPEDANCE AND THE ZAK PHASE WITH THE INTERFACE STATES

In the main text and this Appendix, we have given several examples showing the interface states in two semi-infinite 2D PCs. Using scattering theory, the surface impedance $Z(\omega,k_{||})$ of the semi-infinite PC can be obtained. The signs of $\mathrm{Im}(Z(\omega,k_{||}))$ in the gaps of the projected band structure above and below the quasilongitudinal band are always opposite. For a specific $k_{||}$, in the $\mathrm{Im}(Z(\omega,k_{||})) < 0$ region, the value of $\mathrm{Im}(Z(\omega,k_{||}))$ decreases monotonically from 0 to $-\infty$ with increasing frequency, while in the $\mathrm{Im}(Z(\omega,k_{||})) > 0$ region, the value of $\mathrm{Im}(Z(\omega,k_{||}))$ decreases monotonically from $+\infty$ to 0 with increasing frequency. This implies that $\mathrm{Im}(Z(\omega,k_{||}))$ in the common band gaps between two quasilongitudinal bands of two PCs can always satisfy the condition of interface state formation, and hence the existence of one and only one interface state shown in Figs. 5–8 can be explained. For other common band gaps, as long as they satisfy the $\mathrm{Im}(Z(\omega,k_{||})) < 0$ and $\mathrm{Im}(Z(\omega,k_{||})) > 0$ on either side of the interface, the interface wave existence condition can also be satisfied. Therefore, the interface states must exist (as shown in Figs. 7 and 8). If we know the Zak phases of the bulk band, we do not need to go through the tedious calculation of the scattering problem to obtain $Z(\omega,k_{||})$. Using the band structure information calculated by one unit cell, we can get the Zak phases of the bulk bands, which can determine the characters of the band gaps, and then the existence of the interface states can also be determined. The Zak phase links the bulk band properties to the scattering theory which determines surface properties.

[1] A. H. C. Neto, F. Guinea, N. M. R. Peres, K. S. Novoselov, and A. K. Geim, Rev. Mod. Phys. **81**, 109 (2009).
[2] K. S. Novoselov, A. K. Geim, S. V. Morozov, D. Jiang, M. I. Katsnelson, I. V. Grigorieva, S. V. Dubonos, and A. A. Firsov, Nature (London) **438**, 197 (2005).
[3] Y. Zhang, Y. W. Tan, H. L. Stormer, and P. Kim, Nature (London) **438**, 201 (2005).
[4] R. A. Sepkhanov, Y. B. Bazaliy, and C. W. J. Beenakker, Phys. Rev. A **75**, 063813 (2007).
[5] T. Ochiai, and M. Onoda, Phys. Rev. B **80**, 155103 (2009).
[6] S. Raghu and F. D. M. Haldane, Phys. Rev. A **78**, 033834 (2008).
[7] F. D. M. Haldane and S. Raghu, Phys. Rev. Lett. **100**, 013904 (2008).

[8] J. Mei, Y. Wu, C. T. Chan, and Z. Q. Zhang, Phys. Rev. B **86**, 035141 (2012).
[9] K. Sakoda, J. Opt. Soc. Am. B **29**, 2770 (2012).
[10] K. Sakoda, Opt. Express **20**, 25181 (2012).
[11] X. Huang, Y. Lai, Z. H. Hang, H. Zheng, and C. T. Chan, Nat. Mater. **10**, 582 (2011).
[12] F. Liu, Y. Lai, X. Huang, and C. T. Chan, Phys. Rev. B **84**, 224113 (2011).
[13] M. Silveirinha and N. Engheta, Phys. Rev. Lett. **97**, 157403 (2006).
[14] R. Liu, Q. Cheng, T. Hand, J. J. Mock, T. J. Cui, S. A. Cummer, and D. R. Smith, Phys. Rev. Lett. **100**, 023903 (2008).
[15] B. Edwards, A. Alu, M. E. Young, M. Silveirinha, and N. Engheta, Phys. Rev. Let. **100**, 033903 (2008).
[16] R. W. Ziolkowski, Phys. Rev. E **70**, 046608 (2004).
[17] S. Enoch, G. Tayeb, P. Sabouroux, N. Guerin, and P. Vincent, Phys. Rev. Lett. **89**, 213902 (2002).
[18] A. Alu, M. G. Silveirinha, A. Salandrino, and N. Engheta, Phys. Rev. B **75**, 155410 (2007).
[19] J. Hao, W. Yan, and M. Qiu, Appl. Phys. Lett. **96**, 101109 (2010).
[20] Y. Jin and S. He, Opt. Express **18**, 16587 (2010).
[21] V. C. Nguyen, L. Chen, and K. Halterman, Phys. Rev. Lett. **105**, 233908 (2010).
[22] F. J. Lawrence, L. C. Botten, K. B. Dossou, R. C. McPhedran, and C. M. de Sterke, Phys. Rev. A **82**, 053840 (2010).
[23] F. J. Lawrence, L. C. Botten, K. B. Dossou, C. M. de Sterke, and R. C. McPhedran, Phys. Rev. A **80**, 023826 (2009).
[24] Z. Wang, Y. Chong, J. D. Joannopoulos, and M. Soljacic, Nature (London) **461**, 772 (2009).
[25] M. C. Rechtsman, J. M. Zeuner, Y. Plotnik, Y. Lumer, D. Podolsky, F. Dreisow, S. Nolte, M. Segev, and A. Szameit, Nature (London) **496**, 196 (2013).
[26] A. B. Khanikaev, S. H. Mousavi,W. K. Tse, M. Kargarian, A. H. MacDonald and G. Shvets, Nat. Mater. **12**, 233 (2013).
[27] L. Lu, L. Fu, J. D. Joannopoulos, and M. Soljacic, Nat. Photon. **7**, 294 (2013).
[28] K. Fang, Z. Yu, and S. Fan, Nat. Photon. **6**, 782 (2012).
[29] M. Hafezi, E. A. Demler, M. D. Lukin, and J. M. Taylor, Nat. Phys. **7**, 907 (2011).
[30] Z. Wang, Y. D. Chong, J. D. Joannopoulos, and M. Soljacic, Phys. Rev. Lett. **100**, 013905 (2008).
[31] Z. Yu, G. Veronis, Z. Wang, and S. Fan, Phys. Rev. Lett. **100**, 023902 (2008).
[32] Y. E. Kraus, Y. Lahini, Z. Ringel, M. Verbin, and O. Zilberberg, Phys. Rev. Lett. **109**, 106402 (2012).
[33] Y. Poo, R. X. Wu, Z. Lin, Y. Yang, and C. T. Chan, Phys. Rev. Lett. **106**, 093903 (2011).
[34] Y. Plotnik, M. C. Rechtsman, D. Song, M. Heinrich, J. M. Zeuner, S. Nolte, Y. Lumer, N. Malkova, J. Xu, A. Szameit, Z. Chen and M. Segev, Nat. Mater. **13**, 57 (2014).
[35] M. C. Rechtsman, Y. Plotnik, J. M. Zeuner, D. Song, Z. Chen, A. Szameit, and M. Segev, Phys. Rev. Lett. **111**, 103901 (2013).
[36] J. Zak, Phys. Rev. Lett. **62**, 2747 (1989).
[37] M. Xiao, Z. Q. Zhang, and C. T. Chan, Phys. Rev. X **4**, 021017 (2014).
[38] Y. S. Zhou, B. Y. Gu, and F. H. Wang, J. Phys.: Condens. Matter **15**, 4109 (2003).
[39] C. Guan and L. Yuan, J. Phys. D: Appl. Phys. **41**, 015101 (2008).
[40] M. Mehrabi, A. Soltani-Vala, and J. Barvestani, Opt. Commun. **284**, 5444 (2011).
[41] J. D. Joannopoulos, S. G. Johnson, J. N. Winn, R. D. Meade, *Photonic Crystals: Molding the Flow of Light*, 2nd ed. (Princeton University Press, Princeton, NJ, 2008).
[42] L. L. Lin and Z. Y. Li, Phys. Rev. B **63**, 033310 (2001).
[43] W. Kohn, Phys. Rev. **115**, 809 (1959).
[44] R. Resta, J. Phys.: Condens. Matter. **12**, R107 (2000).
[45] K. Sakoda, *Optical Properties of Photonic Crystals*, 2nd ed. (Springer, Berlin, 2004).